First observation of the splittings of the $E1$ p-wave amplitudes in low energy deuteron photodisintegration and its implications for the Gerasimov-Drell-Hearn Sum Rule integrand

M. A. Blackston,* M. W. Ahmed, B. A. Perdue, and H. R. Weller
Department of Physics, Duke University, Durham, North Carolina 27708, USA and Triangle Universities Nuclear Laboratory, Durham, North Carolina 27708, USA

B. Bewer, R. E. Pywell, and W. A. Wurtz
Department of Physics and Engineering Physics, University of Saskatchewan, Saskatoon, Saskatchewan, Canada S7N 5E2

R. Igarashi
Canadian Light Source, University of Saskatchewan, Saskatoon, Saskatchewan, Canada S7N 0X4

S. Kucuker, B. Norum, and K. Wang
Department of Physics, University of Virginia, Charlottesville, Virginia 22904, USA

J. Li, S. F. Mikhailov, V. G. Popov, and Y. K. Wu
Department of Physics, Duke University, Durham, North Carolina 27708, USA and Duke Free Electron Laser Laboratory, Duke University, Durham, North Carolina 27708, USA

B. D. Sawatzky
Department of Physics, Temple University, Philadelphia, Pennsylvania 19122, USA and Thomas Jefferson National Accelerator Facility, Newport News, Virginia 23606, USA

(Received 10 April 2008; revised manuscript received 16 July 2008; published 17 September 2008; corrected 25 November 2008)

Angular distributions of the cross section and linear analyzing powers have been measured for the $d(\vec{\gamma}, n)p$ reaction at the High Intensity γ-ray Source with linearly polarized beams of 14 and 16 MeV. The outgoing neutrons were detected using the Blowfish detector array, consisting of 88 liquid scintillator detectors with large solid angle coverage. The amplitudes of the reduced transition matrix elements were extracted by means of fits to the data and good agreement was found with a recent potential model calculation of the splittings of the triplet p-wave amplitudes. The extracted amplitudes are used to reconstruct the Gerasimov-Drell-Hearn sum rule integrand for the deuteron and are compared to theory.

DOI: 10.1103/PhysRevC.78.034003 PACS number(s): 24.70.+s, 11.55.Hx, 25.20.Dc, 27.10.+h

I. INTRODUCTION

The study of the photodisintegration of the deuteron has provided one of the simplest systems for examining many aspects of the strong interaction in great detail. This is due to the fact that the electromagnetic interaction is well understood and provides a clean probe of nuclear systems. Potential model calculations, which make use of realistic nucleon-nucleon potentials, are able to explore the role of meson exchange and isobar (e.g., the Δ) currents and of relativistic effects in the photodisintegration reaction. The problem can also be studied using the techniques of effective field theory where power counting provides information on the accuracy of the calculations.

This reaction is known to be dominated by electric dipole ($E1$) transitions at energies just above photodisintegration threshold. In fact, at the energies of the experiment described in this work, about 95% of the total cross section comes from isovector $E1$ transitions to the triplet p waves in the outgoing state. The three p waves, with spin and orbital angular momentum quantum numbers of 1, correspond to total angular momenta in the final state of $J = 0, 1$, and 2. Although the overall p-wave strength has been well studied, the relative strengths or splittings of these three amplitudes have not been measured prior to this work.

This reaction has also received considerable interest recently [1,2] in the context of the Gerasimov-Drell-Hearn (GDH) sum rule [3,4] for the deuteron. The GDH sum rule relates the helicity-dependent photoabsorption cross section difference to the anomalous magnetic moment of the deuteron. It is given by the expression

$$I_{\mathrm{GDH}} = \int_{\omega_{th}}^{\infty} \frac{\sigma_P - \sigma_A}{\omega}\, d\omega = \frac{4\pi^2\alpha}{m^2}\kappa^2 S, \qquad (1)$$

where σ_P and σ_A stand for the photoabsorption cross sections for circularly polarized γ-ray beam and longitudinally polarized target with spins parallel and antiparallel, respectively. The integral over energy, ω, runs from photodisintegration threshold, ω_{th}, to infinity, and the result is simply related to the fine structure constant, α, and the deuteron's mass, anomalous

*Presently at Oak Ridge National Laboratory.

magnetic moment, and spin that are denoted by m, κ, and S, respectively. By virtue of the difference that appears in the integrand, this sum rule highlights the spin dependence of the photoabsorption cross section.

Because the anomalous magnetic moment of the deuteron is so small ($\kappa = -0.143$ [5]) compared to that of the nucleons, a small sum rule value of $I_{\mathrm{GDH}} = 0.65\mu b$ is expected for the deuteron. This is particularly interesting in view of the fact that above pion production threshold, the absorption process on the deuteron can be approximated as being quasi-free reactions with the individual nucleons [1]. Summing the sum rule values for the free proton and neutron gives an expected contribution of about $438\mu b$ above pion threshold. Therefore, if the small sum rule value for the deuteron is to be realized, a nearly equivalent negative contribution must be present below pion threshold.

As predicted by a recent potential model calculation from Schwamb and Arenhövel [1,6,7] (referred to here as the SAPM calculation), all of this negative strength comes at energies very near photodisintegration threshold, due to the contribution from isovector magnetic dipole ($M1$) transitions through the ${}^1s_0$ quasibound state, which can be reached only when the beam and target spins are antiparallel. An indirect determination of this strength was recently published [8]. These calculations also reveal that relativistic effects, most importantly the relativistic spin-orbit current, are responsible for causing the cross-section difference ($\Delta\sigma = \sigma_P - \sigma_A$) to change signs from negative to positive at an energy predicted to be just less than 8 MeV. Without the inclusion of these relativistic contributions, the sum rule value below pion threshold is too negative to offset the high energy positive contribution.

Therefore, an experimental confirmation of a positive GDH strength in this energy region has important implications for the validity of the sum rule for the deuteron. In this work, a photodisintegration measurement performed with linearly polarized photons and unpolarized target at 14 and 16 MeV is described. Fits were performed to extract the reduced transition matrix element (TME) amplitudes, and excellent agreement was obtained with the SAPM calculation for the $E1$ p-wave amplitudes. The implications for the GDH integrand are addressed using an expression for σ_P-σ_A in terms of the amplitudes.

II. DESCRIPTION OF THE EXPERIMENT

The present experiment took advantage of the relatively new High Intensity γ-ray Source (HIγS) and the large solid-angle coverage of a newly constructed segmented neutron detector array (Blowfish) to make precision measurements of the $d(\vec{\gamma}, n)p$ reaction at 14 and 16 MeV [9].

The HIγS facility [10] can produce nearly 100% horizontally polarized γ rays that are nearly monoenergetic ($dE/E \sim 5\%$ in the present case) by Compton backscattering a free-electron laser from highly relativistic electrons in the Duke storage ring. The pulsed nature of the HIγS beams allowed time-of-flight techniques to be used to reduce non-beam-related backgrounds and to identify neutrons from the photodisintegration reaction.

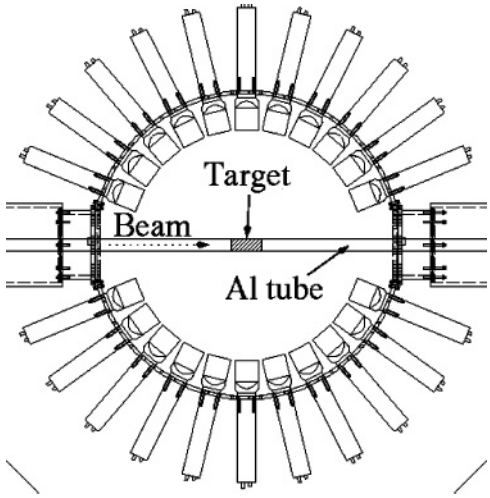

FIG. 1. A drawing of the cross section of the Blowfish detector array. Only two of the eight arms are shown. Some of the Blowfish support structure can also be seen, including the thin aluminum tube that held the target in place.

After being collimated to a size of 2.5 cm in diameter, the beam was incident on a target that consisted of a thin-walled 4.7-cm-long plastic container filled with heavy water (D_2O). An identical H_2O target was used to study backgrounds, which were found to be negligible. Collimated beam-on-target fluxes for this experiment were on the order of $10^5\gamma/s$. The target was held in place by means of a thin aluminum tube that was centered on the beam axis (see Fig. 1).

The Blowfish detector array consists of 88 liquid scintillator (BC-505) neutron detectors positioned spherically around the target location at a radial distance of 16 inches from the target center. The array provides large angular coverage (about 25% of the 4π solid angle), allowing the detailed shape of the angular distribution of the polarized cross section to be measured. The detectors are mounted on 8 semicircular arms equally spaced by $\Delta\phi = 45^\circ$, with 11 detectors per arm. Coverage in θ extends from 22.5° to 157.5° with $\Delta\theta = 13.5^\circ$. In addition, the entire array rotates as a rigid body around the beam axis, allowing systematic effects to be canceled by performing periodic rotations of the array in multiples of 45° in ϕ.

The liquid scintillator detectors allow pulse-shape discrimination (PSD) to be employed for distinguishing neutrons from γ rays that enter the detectors. A gain monitoring system was used to carefully monitor the gains of each detector on a run-by-run basis. Each detector received a pulse of light of constant amplitude from a light-emitting diode (LED), allowing the relative gains to be determined by measuring the relative position of the centroid of the LED spectrum for each run. The absolute gain was then determined by relating the centroid positions to those obtained during a run with a ^{232}Th source placed at the center of the array where the gains are directly measured.

III. DATA REDUCTION

The data were first reduced via PSD to distinguish neutron signals from any other signals. PSD was performed by

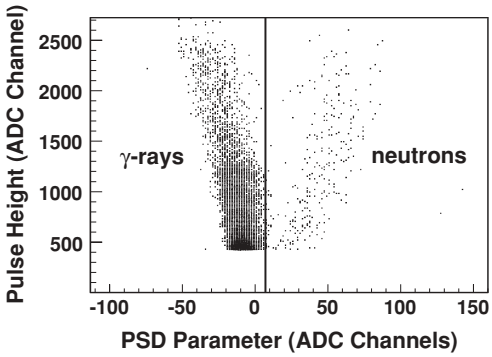

FIG. 2. A PSD spectrum with the applied cut indicated by the vertical line. These data are taken from a single detector over the course of a single 1-h runs.

sending two copies of the detector signals to analog-to-digital converters (ADCs) that integrated the charge in the signal over two different time gates. Almost the entire pulse was integrated for the first copy (long gate), and the second copy was integrated only over approximately the first 30 ns of the pulse (short gate). The PSD parameter is defined as the difference between the two values and highlights the features of the tails of the signals. A plot of the pulse height or long gate value versus the PSD parameter separated out the neutron signals from signals with faster decay times (see Fig. 2).

Next, a common pulse height cut was applied to all the detectors after they were gain matched. This software threshold was applied at a value larger than the highest constant-fraction discriminator (CFD) threshold for any detector, the purpose of which was to ensure that each detector had the same threshold and thus the same efficiency for detecting neutrons. After each of these cuts, the neutrons were easily identified by looking at the resulting time-of-flight (TOF) spectrum. Figure 3 shows the TOF spectrum for both vertical and horizontal detectors before and after the PSD and pulse height cuts. Due to the polarization of the γ-ray beam and the dominance of electric dipole ($E1$) transitions at these energies, the preponderance of events occur in the horizontal detectors and very few are observed in the vertical ones.

The raw neutron yields were then obtained by summing the counts in the TOF spectrum with a timing corresponding to that which is expected for neutrons of interest based on the kinematics of the reaction. Another timing window was also summed in a timing region unrelated to these neutrons to subtract random background.

The angular distribution of the raw yields can be used to construct the two observables in a measurement with linearly polarized beams and unpolarized target: the unpolarized differential cross section, $\sigma(\theta)$, and the linear analyzing power, $\Sigma(\theta)$. $\Sigma(\theta)$ is defined as

$$\Sigma(\theta) = \frac{1}{P_\gamma} \frac{\sigma(\theta, \phi = 0^\circ) - \sigma(\theta, \phi = 90^\circ)}{\sigma(\theta, \phi = 0^\circ) + \sigma(\theta, \phi = 90^\circ)}, \tag{2}$$

where P_γ is the fraction of linear polarization in the beam and $\sigma(\theta, \phi)$ is the polarized differential cross section. $\phi = 0^\circ$ is defined as being the plane of the beam polarization. The

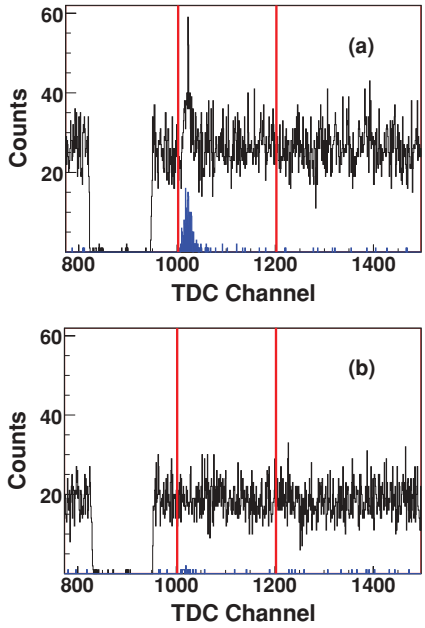

FIG. 3. (Color online) TDC spectra before and after PSD and PH cuts for detectors at $\theta = 90^\circ$ oriented (a) horizontally (in the plane of polarization of the γ-ray beam) and (b) vertically (perpendicular to the plane of polarization). The black histograms are the TDC spectra before PSD and PH cuts are applied and the blue solid histograms [barely visible in (b)] are the spectra after these cuts are applied. The vertical red lines mark the TDC window that was used to accept neutron events. This window was applied to the PSD and PH filtered spectra in blue. These spectra are from single detectors at $\theta = 90^\circ$ and from a single run.

beams at HIγS have polarizations that are consistent with the value of 1.0 [10].

The angular distribution of the unpolarized cross section was determined by summing the yields in the detectors located at a common θ over all ϕ angles, thus integrating out the beam polarization dependence. Absolute beam flux values were not obtained in this measurement, so the unpolarized cross section remains unnormalized.

Because the Blowfish detector array rotated about the beam axis, the analyzing power can be constructed in terms of detector yields in a way that cancels many of the systematic effects. For example, for a set of four orientations of the Blowfish array with detectors A, B, C, and D located in the horizontal plane for Runs 1, 2, 3, and 4, respectively (see Fig. 4 for examples for Runs 1 and 2), the analyzing power can be written in terms of the geometric means as

$$\Sigma(\theta) = \frac{1 - R(\theta)}{1 + R(\theta)} \tag{3}$$

with

$$R = \sqrt[4]{\frac{A_1^H B_2^H C_3^H D_4^H}{A_2^V B_1^V C_4^V D_3^V}}. \tag{4}$$

In this expression, A_1^H stands for the yield in detector A when it is horizontal during Run 1, B_1^V is the yield in detector B when it is vertical during Run 2, and so on.

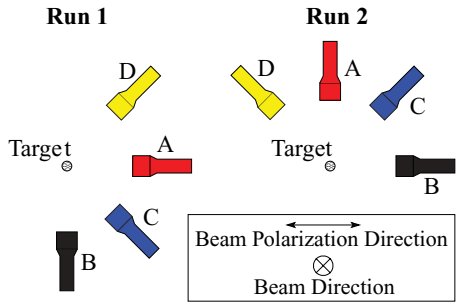

FIG. 4. (Color online) Schematic of the detector location relative to the polarization plane for a pair of array orientations used to construct the analyzing power. From Run 1 to Run 2, the black detector, labeled B, moves from a vertical position, labeled V, to a horizontal position, labeled H. The red detector, labeled A, moves from a horizontal position to a vertical position. Detectors C and D are placed in the horizontal plane for Runs 3 and 4, respectively.

Note that because the yields from a given detector appear in both the numerator and the denominator of Eq. (4), any systematic effects such as detector efficiency will drop out for the analyzing power calculation.

IV. DATA CORRECTIONS

A Monte Carlo simulation was developed using the GEANT4 simulation toolkit [11] to correct for effects such as multiple scattering and finite geometry of the target and detectors. This was done by generating neutrons in the target volume and altering their initial direction and energy according to the resulting angular distribution from the photodisintegration reaction until the simulated data obtained from GEANT4 matched the experimental yields.

The experimental yields from several runs were combined via a geometric mean as described above. Then, using the symmetry of the polarized reaction, the 88 yields corresponding to the 88 detector positions were reduced to 44 yields by averaging yields for detector positions that shared a common θ but were 180° apart in ϕ. Thus the fits to the data consisted of matching 44 simulated yields to the same number of experimental yields.

The cross section that was input into GEANT4 was parametrized in terms of associated Legendre polynomials according to

$$\sigma(\theta,\phi) = A_0 \left[1 + \sum_{k=1} a_k P_k(\cos\theta) + \sum_{k=2} e_k P_k^2(\cos\theta)\cos 2\phi \right], \quad (5)$$

where the P_k and P_k^2 functions are the associated Legendre polynomials, and the a_k and e_k coefficients are parameters that were varied. The A_0 parameter sets the overall scale of the total cross section, σ_T, via $\sigma_T = 4\pi A_0$. Because the absolute value of the cross section was not obtained from this measurement, A_0 was simply a scale factor, which was ultimately set to 1.0.

The fits were performed using the fitting routine MINUIT [12], and it was found that satisfactory fits to the yields were obtained with an expansion containing $k \leqslant 4$. The χ^2 values of these fits (see Tables I and II) indicated that additional terms were not statistically justified. The Legendre polynomial coefficients extracted from the fits are reported in Tables I and II. Finally, the observables were corrected by applying a factor to each data point consisting of the ratio of the observables based on the cross section that was input into GEANT4 to the outputted simulated observables from GEANT4.

TABLE I. Legendre polynomial coefficients extracted from fits to the 14-MeV data. SAPM stands for the Schwamb Arenhövel potential model calculation [1,6,7]. Note that the A_0 coefficient is 1.0 by definition. The reduced χ^2 value (χ^2/ndf) for this fit was 0.99.

		Stat.	Syst.	SAPM
a_1	−0.056	±0.006	±0.005	−0.134
a_2	−0.860	±0.009	±0.008	−0.926
a_3	0.068	±0.011	±0.008	0.128
a_4	−0.041	±0.014	±0.018	−0.012
e_2	0.450	±0.002	±0.002	0.463
e_3	−0.011	±0.001	±0.001	−0.021
e_4	0.005	±0.001	±0.001	0.001

The results for the observables are shown in Figs. 5 and 6 where they are compared to the SAPM and a fit in terms of the transition matrix elements, which is described below. The systematic errors on the data points were estimated to be of the same order of magnitude as the statistical errors (size of the dots in some cases) shown in the figures. Tables III and IV report the corrected data in tabular form.

It should be noted that for the 16-MeV runs, all the detectors located at $\theta = 63°$ and 76° exhibited an effective gain shift that could not be accounted for using the gain monitoring system. Each of these detectors shared a common power supply which is a possible culprit for the problem. Although the resulting effects would cancel out in the case of the analyzing power, the same is not true in the case of the angular distribution of the unpolarized cross section. Therefore, these data points were discarded from the analysis of the 16-MeV data.

The data for the unpolarized cross section from both beam energies exhibit a symmetry about $\theta = 90°$, whereas the

TABLE II. Legendre polynomial coefficients extracted from fits to the 16 MeV data. SAPM stands for the Schwamb Arenhövel potential model calculation [1,6,7]. Note that the A_0 coefficient is 1.0 by definition. The reduced χ^2 value (χ^2/ndf) for this fit was 0.99.

		Stat.	Syst.	SAPM
a_1	−0.077	±0.006	±0.012	−0.146
a_2	−0.855	±0.009	±0.026	−0.912
a_3	0.089	±0.013	±0.044	0.137
a_4	−0.034	±0.014	±0.030	−0.014
e_2	0.446	±0.002	±0.004	0.455
e_3	−0.014	±0.001	±0.003	−0.023
e_4	0.004	±0.001	±0.002	0.001

TABLE III. Corrected cross section and analyzing power values for the 14-MeV data. All values are given in the center-of-mass frame.

$\theta_{\text{c.m.}}$	σ/A_0	Stat.	Syst.	Σ	Stat.	Syst.
24.0°	0.321	±0.010	±0.014	0.704	±0.032	±0.019
38.2°	0.602	±0.012	±0.010	0.854	±0.014	±0.010
52.4°	0.930	±0.011	±0.018	0.890	±0.007	±0.009
66.4°	1.150	±0.014	±0.018	0.933	±0.004	±0.007
80.2°	1.345	±0.013	±0.019	0.915	±0.004	±0.005
93.8°	1.444	±0.018	±0.018	0.927	±0.005	±0.005
107.2°	1.361	±0.015	±0.013	0.940	±0.008	±0.006
120.4°	1.176	±0.014	±0.014	0.933	±0.004	±0.007
133.4°	0.875	±0.012	±0.017	0.948	±0.010	±0.007
146.2°	0.568	±0.012	±0.014	0.856	±0.011	±0.014
159.0°	0.301	±0.009	±0.017	0.692	±0.026	±0.033

theory predicts a slight backward peaking. The TME analysis indicates that this difference can be attributed to the difference between the $E2$ d-wave strengths extracted from the data and those predicted by the theory. Although the d waves comprise only a few percent of the total cross section, they interfere with the dominant $E1$ p waves to give rise to the predicted fore-aft asymmetry.

V. TRANSITION MATRIX ELEMENT ANALYSIS

Using the formalism of Ref. [13], the polarized differential cross section can be written in terms of the amplitudes and phases of the reduced TMEs that contribute to the reaction at these energies. The reduced TMEs represent the strength of the transition and are dependent on only the radial part of the TMEs, with the angular part factored out. The TMEs are labeled by the electric or magnetic multipole responsible for the transition (i.e., $E1$, $M1$, $E2$, etc.), and the quantum numbers of the outgoing n-p system using the notation ${}^{2s+1}l_J$. The channel spin is denoted by s, which for two spin 1/2 particles can take on values of 0 or 1, l is the orbital angular momentum in spectroscopic notation (s waves are $l = 0$, p waves are $l = 1$, d waves are $l = 2$, etc.), and J is the total angular momentum, $\vec{l} + \vec{s}$.

Selection rules allow some of the TMEs to be omitted from the fits because they are expected to be negligible. For instance, negligible amplitudes are expected from the $E1$ ${}^1p_1$ and $E2$ ${}^1d_2$ terms, because they correspond to "spin-flip" electric transitions. The same is true of the $M1$ ${}^3s_1$ term because it has the same quantum numbers as the ground state of the deuteron, making it negligible due to orthogonality. Indeed, theory predicts that each of these amplitudes is at least three orders of magnitude down in strength compared to the weakest amplitude included in our fits [14].

Using these and similar considerations along with guidance from the SAPM calculation and limiting ourselves to $M1$, $E1$, and $E2$ multipoles and partial waves less than or equal to $l = 2$, the following TMEs were considered: $(M1)^1s_0$, $(E1)^3p_0$, $(E1)^3p_1$, $(E1)^3p_2$, $(E2)^3d_1$, $(E2)^3d_2$, and $(E2)^3d_3$. It should be noted that the $M1$ and $E1$ transitions considered here are isovector, whereas the $E2$ transitions are isoscalar. Ultimately, the simplifications required to limit ourselves to these seven terms will be tested by our ability to describe the data.

The relative phases of the TMEs were fixed by using Watson's theorem [15], which identifies the TME phases with the n-p scattering phase shifts. This identification is valid as long as there are no other open reaction channels and if the mixing between orbital angular momentum states is small. Both conditions are met for the energies of this experiment. The n-p scattering phase shifts were obtained from the SAID phase shift analysis [16]. The phases used in the present fits

TABLE IV. Corrected cross section and analyzing power values for the 16 MeV data. All values are given in the center-of-mass frame.

$\theta_{\text{c.m.}}$	σ/A_0	Stat.	Syst.	Σ	Stat.	Syst.
24.1°	0.314	±0.013	±0.025	0.737	±0.047	±0.040
38.4°	0.586	±0.012	±0.011	0.829	±0.010	±0.012
52.6°	0.891	±0.012	±0.026	0.892	±0.007	±0.008
94.0°	1.423	±0.016	±0.031	0.921	±0.003	±0.013
107.4°	1.333	±0.031	±0.023	0.925	±0.005	±0.009
120.6°	1.183	±0.018	±0.026	0.917	±0.006	±0.008
133.6°	0.898	±0.011	±0.029	0.902	±0.006	±0.015
146.4°	0.596	±0.009	±0.023	0.836	±0.013	±0.021
159.0°	0.304	±0.006	±0.020	0.677	±0.026	±0.052

TABLE V. n-p scattering phase shifts corresponding to E_γ of 14 and 16 MeV from the SAID analysis [16].

TME	Phase shifts	
	14 MeV	16 MeV
$^3p_0(E1)$	8.6°	9.3°
$^3p_1(E1)$	−4.9°	−5.5°
$^3p_2(E1)$	2.9°	3.4°
$^3d_1(E2)$	−2.9°	−3.6°
$^3d_2(E2)$	4.1°	5.0°
$^3d_3(E2)$	0.1°	0.2°

are listed in Table V. To test the sensitivity of the fits to the accuracy of the phases (which come into the formalism only as phase differences), fits were performed with the phases set to both double and one-half of the values from the SAID analysis. The results indicated a negligible dependence on the values of the phases at this level of accuracy, giving results well within the statistical uncertainties of the extracted parameters.

This left the seven TME amplitudes as free parameters in fits to the data. Even with these simplifications, we are left with seven unknown amplitudes and a total of six independent known quantities. This is due to the fact that although there are five Legendre coefficients from the angular distributions of the cross section and three from the analyzing powers, there also exist two constraint relationships when the coefficients are written in terms of the amplitudes: $a_3 = -6\,e_3$ and

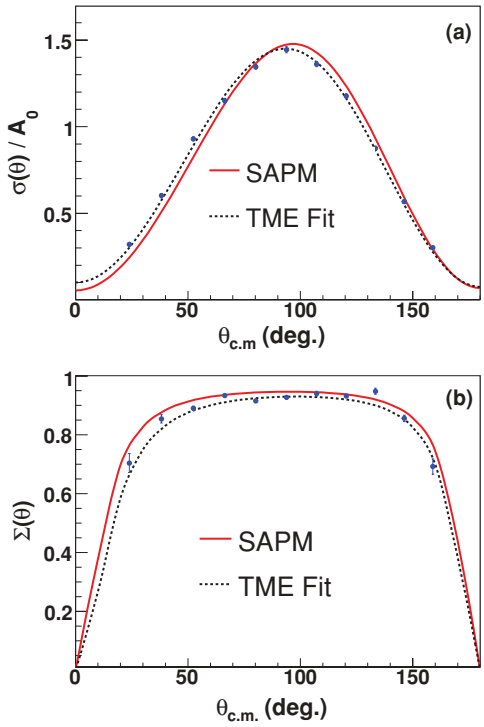

FIG. 5. (Color online) 14 MeV (a) cross section and (b) analyzing power along with fits from the extraction of TME amplitudes. The solid red curves are from the SAPM calculation and the dotted black curves represent the fit to the data. The errors on the data points are statistical only.

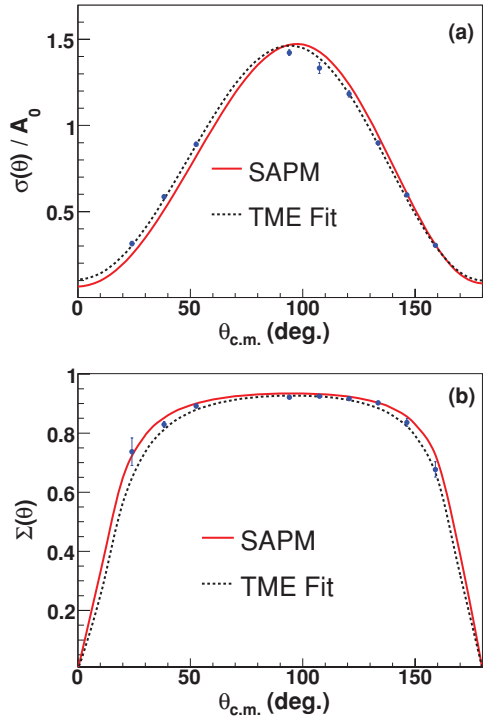

FIG. 6. (Color online) 16 MeV (a) cross section and (b) analyzing power along with fits from the extraction of TME amplitudes. The solid red curves are from the SAPM calculation and the dotted black curves represent the fit to the data. The errors on the data points are statistical only.

$a_4 = -12\,e_4$. This leaves six independent observables. Therefore, to fit the seven unknown amplitudes to the data, an additional constraint is needed. We chose to set the s-wave amplitude equal to the theory value, which is about 1.8% of the total cross-section strength.

It should be noted that the p-wave splitting results discussed below were actually found to be quite robust with regard to the value of the s-wave strength. All three p-wave strengths agreed within error with the best fit values when the s-wave strength was varied between 0% and 6% of the total strength, adding confidence to the split p-wave values being reported.

The fits were performed by expressing the coefficients of the associated Legendre polynomial expansion in terms of the TME amplitudes and fitting to the 44 experimental yields in the same way as described in Section IV. In this case, however, the coefficients in front of the Legendre polynomials took on values that were determined by the values of the TME amplitudes, which were the free parameters. The representation of the fits in terms of the observables are compared with the experimental observables in Figs. 5 and 6.

VI. DISCUSSION OF RESULTS

The set of amplitudes obtained from the fits converged to two distinct solutions depending on the seed values for the amplitudes passed to the fit. A systematic survey was performed using a grid of seed values and indicated that there were no other solutions having comparable χ^2 values. Both solutions

returned identical χ^2 values and neither could be eliminated as a possible solution from the point of view of the fits.

The fits to the data yielded reduced χ^2 values (χ^2/ndf) of 1.8 and 1.7 for the 14- and 16-MeV fits, respectively. These χ^2 values are larger than the values obtained from the Legendre polynomial fits to the data. This is due to the constraints imposed when writing the coefficients in terms of the amplitudes that were included in our analysis. For instance, when the coefficients are expressed in this way, the value of e_3 is fixed according to $a_3 = -6\,e_3$ and e_4 is similarly fixed according to $a_4 = -12\,e_4$. In the case of the Legendre fits, however, each coefficient is allowed to assume any value. Despite the constraints placed on the Legendre coefficients in the fit to extract TME amplitudes, the coefficients obtained from those fits agreed within error with the coefficients extracted from the pure Legendre fits.

It should be noted that because the absolute cross sections were not measured, the leading coefficient of the Legendre polynomial expansion was set equal to 1.0. This means that all of the amplitudes discussed here are normalized amplitudes so that the values shown represent only the relative strengths of the TME amplitudes. The theoretical values have been similarly normalized.

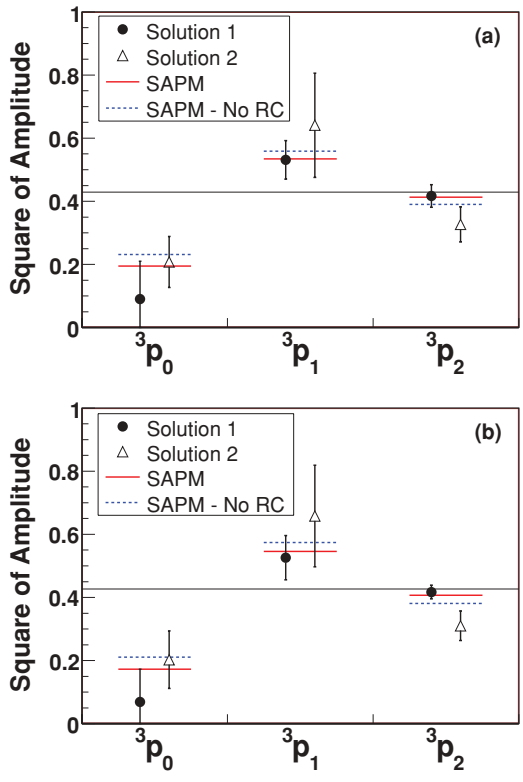

FIG. 7. (Color online) Square of the triplet $E1$ p-wave amplitudes for (a) 14 MeV and (b) 16 MeV as extracted from the data and compared to the SAPM calculation. The solid red line is the prediction from the full SAPM calculation and the dashed blue line is the prediction for the calculation without the inclusion of relativistic contributions (RC). The thin solid line that extends across the entire plot indicates the values that the squares of the amplitudes would have if there no p-wave splitting. Error bars are statistical only.

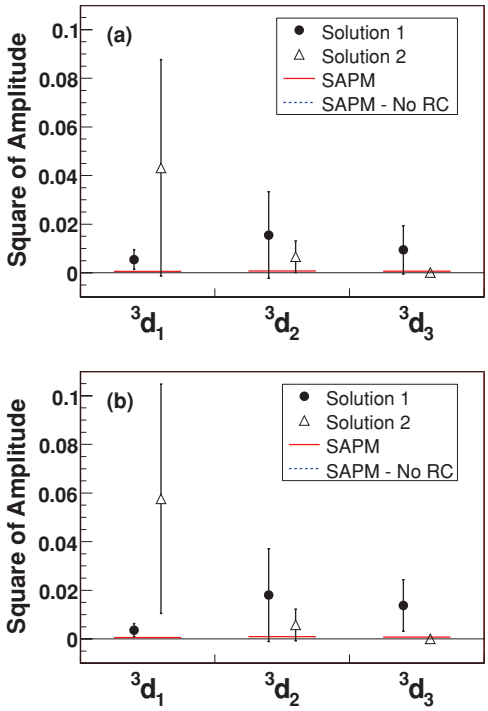

FIG. 8. (Color online) Square of the triplet $E2$ d-wave amplitudes for (a) 14 MeV and (b) 16 MeV as extracted from the data and compared to the SAPM calculation. The solid red line is the prediction from the full SAPM calculation and the dashed blue line is the prediction for the calculation without the inclusion of relativistic contributions (RC). The two theory values are so close that they are indistinguishable. Error bars are statistical only.

The results indicate very good agreement with the SAPM calculation of the triplet $E1$ p-wave amplitudes. The results for the p waves are shown as the square of the normalized amplitudes and compared to the theory in Fig. 7. Also shown in the figure is the SAPM calculation without the inclusion of relativistic currents so the dependence of the p-wave splittings on those effects can be seen. Figure 7 shows that the basic behavior of the splittings predicted by the SAPM is well reproduced by both solutions: i.e., a decrease in the $^3p_0$ term and an increase in the $^3p_1$ term relative to the unsplit values. The additional (small) effect of the relativistic contribution, which causes an increase in the $^3p_2$ term relative to the $^3p_0$ and $^3p_1$ terms, is slightly favored by the set of amplitudes labeled Solution 1 (see the $^3p_2$ amplitude at 16 MeV), although just marginally within the error bars.

Figure 8 shows that the $E2$ d waves take on systematically larger values than expected by the theory for these energies. However, the error bars are so large that most of the points overlap the theoretical values. As already mentioned, the difference in the d waves is responsible for the difference observed in the fore-aft asymmetry between the theory and the data for the unpolarized cross section (see Figs. 5 and 6). Although they are small in magnitude, the d waves interfere with the dominant p-wave amplitudes to affect the angular distribution.

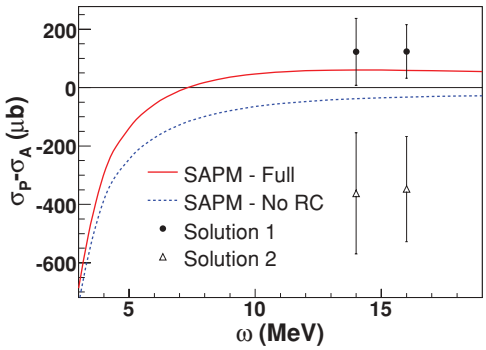

FIG. 9. (Color online) σ_P-σ_A for the two solutions extracted for the TME amplitudes of the reaction at each beam energy. Also shown is the full SAPM calculation and the SAPM calculation without relativistic contributions (RC). Error bars are statistical only.

VII. THE GERASIMOV-DRELL HEARN SUM RULE

Using the formalism of Ref. [17], σ_P-σ_A, which enters into the GDH sum rule integrand, can be written in terms of the TME amplitudes extracted from the fits to the data. At these energies, which are near where the integrand is predicted to change from negative to positive, the cross section difference is determined primarily by the details of the splittings of the $E1$ p waves. Explicitly, when considering the terms we included in our fits to the data, the cross-section difference can be written in terms of the reduced TMEs as

$$\begin{aligned}\Delta\sigma = \tfrac{1}{2}\pi\lambda\!\!\!^{-2}\big[&-|^1s_0(M1)|^2 \\ &-|^3p_0(E1)|^2-\tfrac{3}{2}|^3p_1(E1)|^2+\tfrac{5}{2}|^3p_2(E1)|^2 \\ &-\tfrac{3}{2}|^3d_1(E2)|^2-\tfrac{5}{6}|^3d_2(E2)|^2+\tfrac{7}{3}|^3d_3(E2)|^2\big], \qquad (6)\end{aligned}$$

where $\lambda\!\!\!^{-}$ is written in terms of the γ-ray wavelength, λ, as $\lambda\!\!\!^{-} = \lambda/2\pi$. In the present case, because absolute normalizations were not obtained for the measured cross sections, the cross section difference was normalized using the theoretical value of the total cross section, which agrees with existing data to better than 10%. Note that Eq. (6) indicates that a small increase in the $^3p_2$ amplitude relative to the $^3p_0$ and $^3p_1$ terms will lead to a positive contribution to $\Delta\sigma$ from the p waves. As previously noted, this is exactly the effect of the relativistic contribution.

The results for $\Delta\sigma$ are shown in Fig. 9 for both solutions at each energy. It is clear, by examining the theory curves with and without the relativistic contributions, that $\Delta\sigma$ is very sensitive to small changes in the p-wave splittings shown in Fig. 7. These experimental results were obtained using the p-wave splittings shown in Fig. 7, the d-wave splittings shown in Fig. 8 (which have almost no effect due to their relatively small sizes), and the theory values for the s-wave strength. The details of the splittings of the p-wave amplitudes are responsible for the positive $\Delta\sigma$ values obtained for points labeled Solution 1 in Figure 9.

Although the integrand values designated Solution 2 cannot be ruled out, the Solution 1 values are to be preferred to the Solution 2 values, because the Solution 2 values would contribute to producing a total sum rule value that is much too negative, which would most likely violate the sum rule when integrated over all energies. These results provide the first experimental indication that the GDH integrand is becoming positive above 7 MeV, as predicted by theory. As Fig. 9 demonstrates, the crossover is due to the inclusion of relativistic contributions in the theory that, by virtue of the relativistic spin-orbit current, increases the $^3p_2$ amplitude relative to the $^3p_0$ and $^3p_1$ amplitudes.

VIII. CONCLUSIONS

High-precision measurements of the deuteron photodisintegration reaction were performed near 15 MeV, allowing the extraction of angular distribution of the unpolarized cross section and the linear analyzing power. There are no previous measurements in this energy region that achieve such high precision over such a large angular region.

Until now, the splittings of the p-wave amplitudes for this reaction, which is so fundamental to nuclear physics, have not been observed experimentally. The amplitudes extracted in this work agree well with the recent potential model calculation from Schwamb and Arenhövel [1,6,7] and even suggest the need for including a relativistic contribution at these energies. In addition, the GDH integrand values constructed using one set of the extracted amplitudes agree well with the prediction of the SAPM calculation. The observation of a GDH strength that is becoming positive at these energies has important implications for the validity of the sum rule for the deuteron because of the close connection between the positive value and the relativistic effects that are needed in the calculation to achieve the small sum rule value for the deuteron when integrating over all energies.

It will be interesting to reproduce these positive values in accurate direct measurements of the GDH integrand, which will begin at HIγS in late 2008. However, such measurements will not provide the insight into the origin of the value obtained in the present work.

ACKNOWLEDGMENTS

We thank M. Schwamb for providing the SAPM calculation and for helpful discussions. This work was supported in part by the US Department of Energy, Office of Nuclear Physics, under no. DE-FG02-97ER41033.

[1] H. Arenhövel, A. Fix, and M. Schwamb, Phys. Rev. Lett. **93**, 202301 (2004).
[2] J. Ahrens *et al.*, Phys. Rev. Lett. **97**, 202303 (2006).
[3] S. B. Gerasimov, Sov. J. Nucl. Phys. **2**, 430 (1966).
[4] S. D. Drell and A. C. Hearn, Phys. Rev. Lett. **16**, 908 (1966).
[5] P. Mohr *et al.*, Rev. Mod. Phys. **72**, 351 (2000).
[6] M. Schwamb and H. Arenhövel, Nucl. Phys. **A696**, 556 (2001).

[7] M. Schwamb and H. Arenhövel, Nucl. Phys. **A690**, 682 (2001).
[8] M. W. Ahmed *et al*., Phys. Rev. C **77**, 044005 (2008).
[9] M. A. Blackston, Ph.D. thesis, Duke University (2007).
[10] V. Litvinenko *et al*., Phys. Rev. Lett. **78**, 4569 (1997).
[11] S. Agostinelli *et al*. (GEANT4 Collaboration), Nucl. Instrum. Methods A **506**, 250 (2003).
[12] F. James, CERN, Program Library Long Writeup D506, Version 94.1 (Geneva, Switzerland, 1998).
[13] H. Weller *et al*., At. Data Nucl. Data Tables **50**, 29 (1992).
[14] M. Schwamb (private communication 2007).
[15] L. D. Knutson, Phys. Rev. C **59**, 2152 (1999).
[16] Center for Nuclear Studies, The George Washington University (2007), SAID analysis: http://gwdac.phys.gwu.edu/.
[17] H. Weller *et al*., At. Data Nucl. Data Tables **58**, 219 (1994).